Mon. Not. R. Astron. Soc. **282,** 889–899 (1996)

The emission-line spectrum of the hot R Coronae Borealis star MV Sgr

Gajendra Pandey,[1]★ N. Kameswara Rao[1]★† and David L. Lambert[2]★†

[1] *Indian Institute of Astrophysics, Bangalore 560034, India*
[2] *Department of Astronomy, University of Texas, Austin, TX 78712, USA*

Accepted 1996 May 15. Received 1996 May 9; in original form 1996 January 31

ABSTRACT

Spectra of MV Sgr obtained at CTIO in 1992 May show many emission lines in the red. Most of the emission lines show two components with a minimum centred at the stellar velocity. Species represented include H, He I, Ti II and Fe II. Of special interest is emission in the Li I 6707-Å resonance doublet. [O I] and [N II] emission indicate the presence of a nebula around the star. The radial velocity of the absorption lines (Al III, Si III, N II and C II) and Fe II emission lines agrees with the radial velocity given by Jeffery et al.

Key words: line: profiles – stars: emission-line, Be – stars: individual: MV Sgr.

1 INTRODUCTION

MV Sgr is, with DY Cen and V348 Sgr, one of the select trio of hot R Coronae Borealis stars (RCBs). Its identification as an RCB variable was made by Hoffleit (1958). The spectrum of MV Sgr at maximum light has been described by Herbig (1964, 1975a) as that of a hydrogen-deficient B-type star with several emission lines prominent in the red and attributable to Hα, Fe II, He I, Si II, N I, Ca II and O I. He suggested that the excitation temperature of the Fe II emission region is substantially lower than the colour temperature of the star. Rao & Nandy (1982) noticed low-excitation lines of Fe II, Si II, C I, O I and Al II in absorption in the ultraviolet, and showed that they varied in strength whereas higher excitation absorption lines (e.g. C II, Al III) did not. From the dereddened flux distribution from the visual to the ultraviolet, Drilling et al. (1984) estimated the $T_{\rm eff}$ of the star to be $15\,400 \pm 400$ K.

Based on high-resolution spectra obtained in the blue, Jeffery et al. (1988) analysed the photospheric (absorption) spectrum at maximum light and concluded, from the hydrogen and helium lines, that the star is hydrogen deficient to the same degree as the hot helium star HD 124448 (H/He $< 1 \times 10^{-4}$) but that nitrogen and silicon are underabundant by about a factor of 10 and carbon is down by a factor of about 100 relative to HD 124448. Jeffery et al. also remarked that all Fe II emission lines present in their spectrum are split with a peak separation of 68 km s^{-1}. It was argued that the emitting region was optically thick in the Fe II. Other emission lines were attributed to Mg II, Ca II, Ti II and Si I. Rao, Houziaux & Giridhar (1990) identified forbidden [S II] lines in the blue.

Dust is located near the star. An infrared excess was observed by Feast & Glass (1973), Kilkenny & Whittet (1984) and Walker (1986). The infrared spectrum appears to be a composite of two blackbodies, one at 1600 K and a second at 230–550 K. The distribution of the dust around the star is unknown, but one presumes the 1600-K dust is closer to the star than the 250-K dust.

2 OBSERVATIONS

The present observations were obtained with the 4-m telescope and a CCD-equipped Cassegrain echelle spectrometer at the Cerro Tololo Inter-American Observatory during the night of 1992 May 22–23. Our spectrum covers the wavelength range 5480–6980 Å. The FWHM of the terrestrial [O I] line at 5577 Å in the final co-added spectrum corresponds to 9.0 km s^{-1}, or a resolution of 33 000. This resolution is confirmed by the widths of the Th lines in exposures of a Th–Ar hollow cathode lamp taken immediately following the stellar exposures. The signal-to-noise ratio in the continuum at the peak of the echelle blaze runs from about 80 at 5500 Å to 85 at 6800 Å. The reductions have been done using the RESPECT and IRAF software packages at Bangalore.

★E-mail: pandey@iiap.ernet.in (GP); nkrao@iiap.ernet.in (NKR); dll@astro.as.utexas.edu (DLL).
†Visiting Astronomer Cerro Tololo Inter-American Observatory, operated by AURA under contract with the National Science Foundation.

3 DESCRIPTION OF THE SPECTRUM

The spectrum is a mix of absorption and emission lines. The absorption-line component that we attribute to the stellar photosphere is similar to that described by Jeffery et al. (1988). Absorption lines are mainly due to Al III, Si III, C II (higher multiplets), N II, O II and possibly Ne I. Permitted or forbidden emission lines from the following atoms and ions are readily identifiable: H, He I, Li I, C I, C II, [N II], [O I], Ne I, Na I, Mg I, Si II, Ti II, Fe I, Fe II and Ni I. Table 1 provides a list of the identified emission lines. Diffuse interstellar absorption bands (Herbig 1975b) are seen in the spectrum. The bands at $\lambda\lambda$ 5487, 5780, 5797, 6011, 6196, 6203, 6269, 6376, 6379 and 6613 are clearly present.

Sample portions of the spectrum are provided in Figs 1 and 2 to show the fascinating mix of absorption and emission profiles. Fig. 1 shows an emission line attributed to the Li I 6707-Å doublet and also Ca I 6717 Å along with an absorption line of O II 6721 Å. We believe this is the first astrophysical detection of the Li I resonance feature at 6707 Å in emission. Fig. 2 shows C II ($\lambda\lambda$ 6780, 6784, 6787, 6791, 6798, 6800 and 6812) in absorption and Ni I 6767 Å in emission. Selected emission-line profiles are displayed in Figs 3, 4, 5 and 6. Fig. 3 shows the emission line of Hα, a strong Fe II line, a weak C I line and the prominent Si II at 6347 Å. Fig 4 shows the [N II] and [O I] profiles. Fig. 5 shows a profile of Li I with those of the Ca I] 6572 Å, Fe I 5501 Å, and Ni I 6767 Å.

Profiles of four Fe II lines from the multiplet RMT46 are shown in Fig. 6. The Fe II emission lines clearly show two components with a minimum centred at about the stellar (photospheric) velocity (see below). Weaker lines (Fig. 5) tend to show flat-topped profiles with a width similar to that of the stronger and double-peaked lines. A central minimum may be present, but higher signal-to-noise spectra are needed to derive definitive profiles for these weaker lines.

4 RADIAL VELOCITIES

The absorption lines of Al III, Si III, N II and C II give a velocity of -93 ± 4 km s^{-1}, which we refer to as the stellar velocity. This value agrees well with earlier measurements of -91 ± 7 and -96 ± 4 km s^{-1} given by Jeffery et al. (1988), and one of -95 ± 8 km s^{-1} by Rao et al. (1990). If, as is likely, MV Sgr experiences atmospheric pulsations, their amplitude would seem to be just a few km s^{-1}.

The diffuse interstellar bands at 5796, 6195, 6202 and 6613 give a mean radial velocity of -8 km s^{-1} when rest wavelengths are taken from Herbig (1975b). An absorption component at this velocity is seen in the Na I D lines. Our spectra show that this Na I D component consists of at least two unresolved components. There is another absorption component of the Na I D lines at a radial velocity of 29 km s^{-1}. Jeffery et al. (1988) find an absorption component for Ca II H and K lines at 20 km s^{-1} which they attribute to the interstellar medium. This velocity is consistent with a cloud at approximately 4 kpc.

The emission lines are centred on the stellar velocity. Lines with a clear central minimum between the two emission peaks have their central minimum at -92 ± 5 km s^{-1} (from 20 lines). In cases in which the central minimum is not obvious, the centre of the line coincides with the stellar

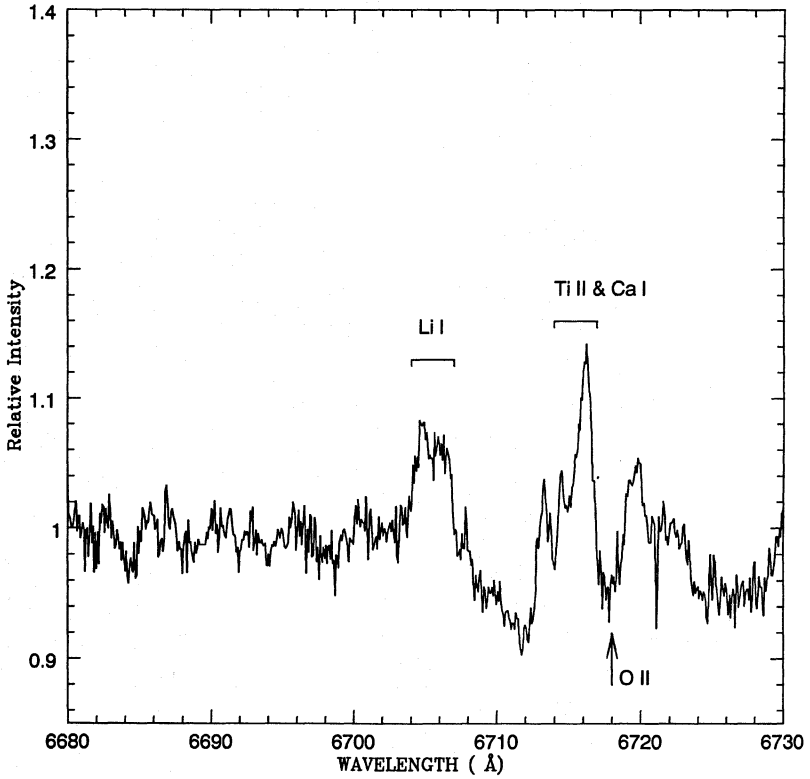

Figure 1. Spectrum of MV Sgr showing the Li I 6707-Å, Ca I and Ti II lines in emission and the O II 6721-Å line in absorption.

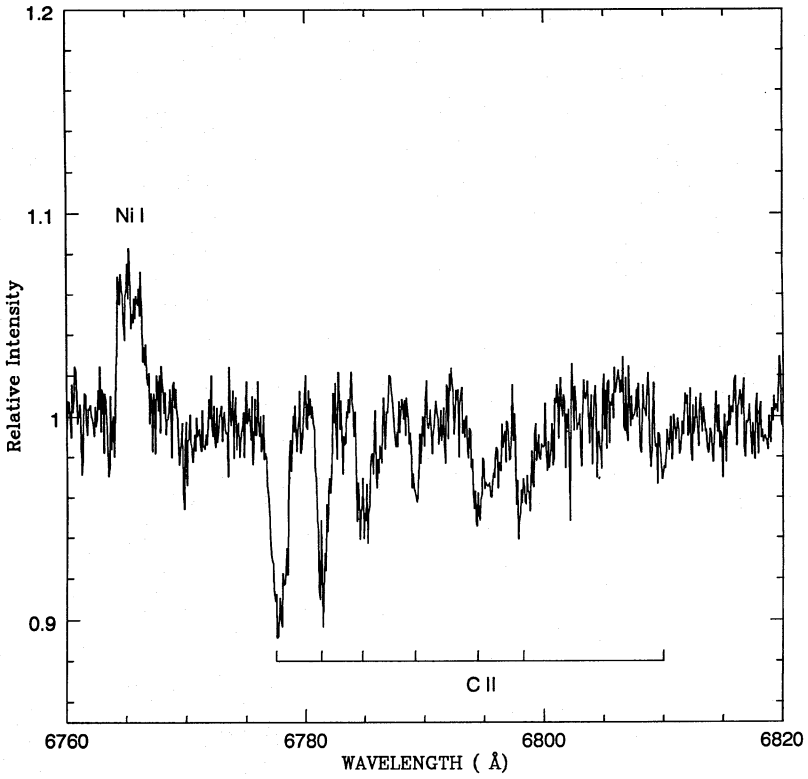

Figure 2. Spectrum of MV Sgr showing the C II (RMT14) absorption lines and Ni I λ6767 emission.

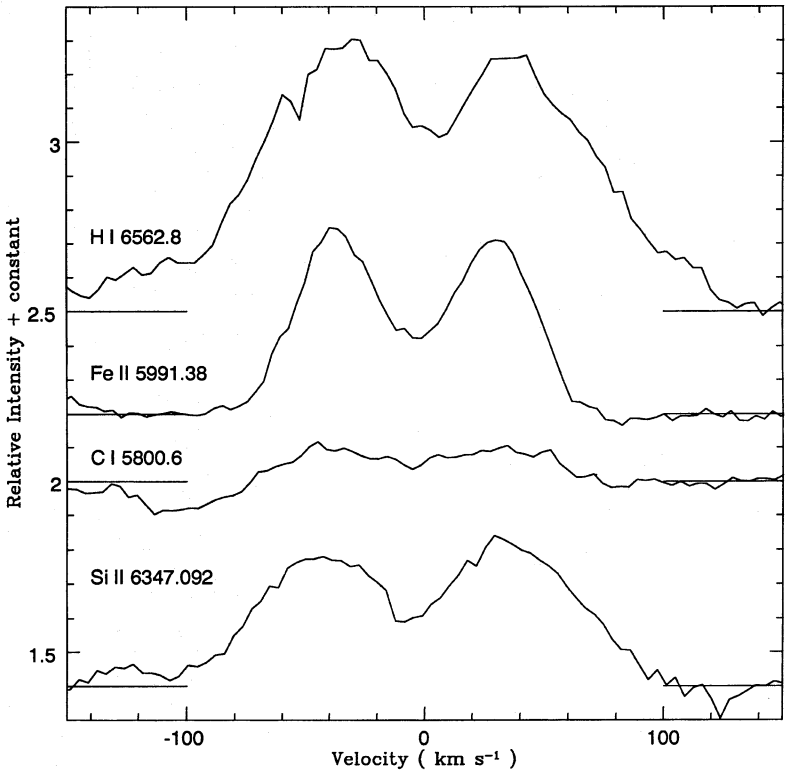

Figure 3. Comparison of emission lines of Hα, Fe II λ5991, C I λ5800 and Si II λ6347. The zero of the velocity scale refers to the photospheric velocity. The position of the mean continuum for each spectrum segment is indicated by the line marked.

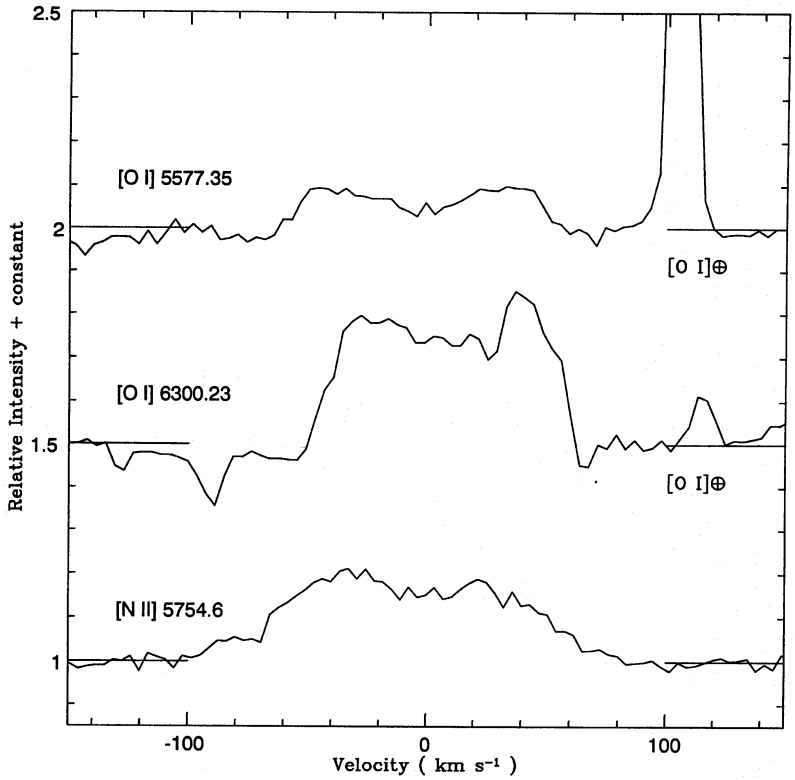

Figure 4. Comparison of forbidden emission lines of O I and N II. The abscissa is similar to Fig. 3. The mean continuum for each spectrum segment is indicated as in Fig. 3.

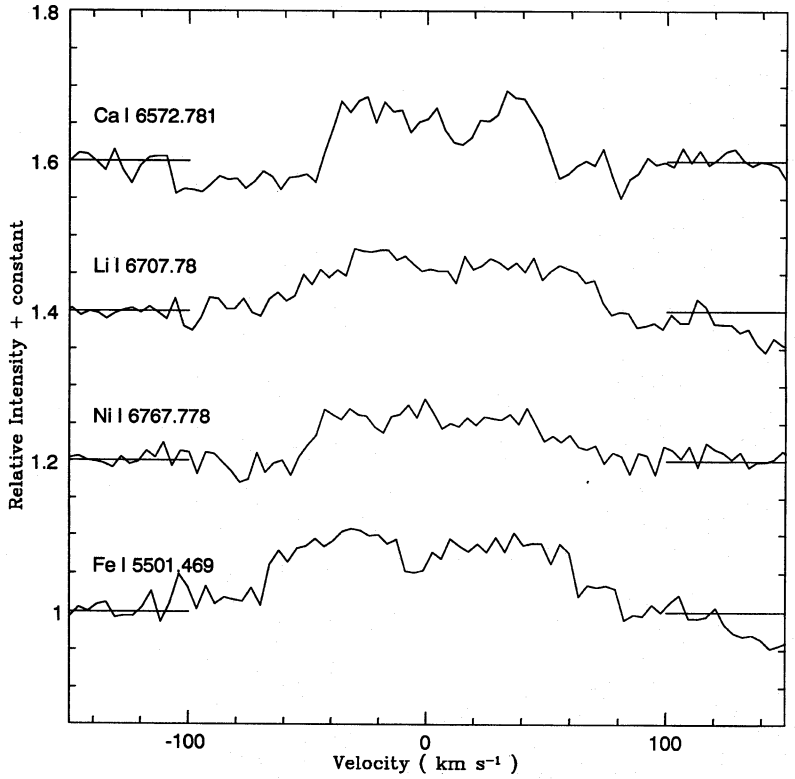

Figure 5. Comparison of Li I 6707-Å emission-line profile and other low-excitation weak permitted lines. The velocity scale is similar to Fig. 4. The mean continuum for each spectrum segment is marked as in Fig. 3.

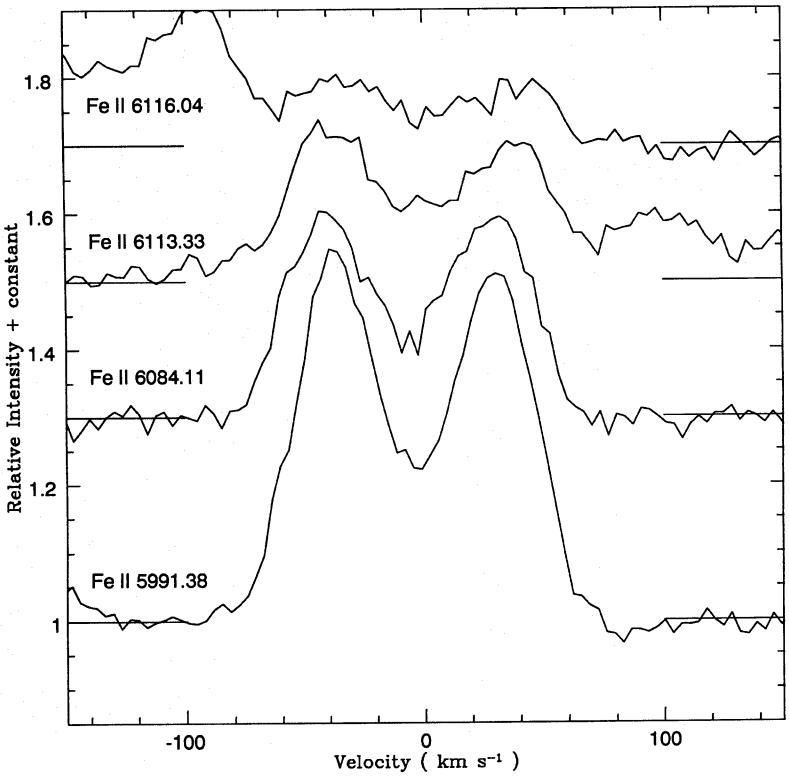

Figure 6. Comparison of Fe II emission lines from RMT46. The velocity scale is similar to Fig. 4. The mean continuum for each spectrum segment is marked as in Fig. 3.

velocity. The velocity separation between the blue and red peaks is 68 ± 4 km s^{-1} from 15 Fe II lines. This splitting agrees with the estimate of 68 km s^{-1} reported by Jeffery et al. (1988). It would seem that the emission-line spectrum has not changed significantly.

5 EMISSION LINES

We have assumed that the split lines are formed from two components, redshifted and blueshifted, which have been measured independently where possible. The measured equivalent widths of the emission lines (both components) have been converted to line fluxes using the *UBVRI* colours from Landolt (1979) to define the continuum flux. A reddening correction of $E(B-V)=0.45$ is adopted from Heber & Schönberner (1981) who compared observed and predicted colours. Drilling et al. (1984) give $E(B-V)=0.38$ based on the strength of the 2200-Å interstellar bump. Our principal conclusions are unaffected by the adoption of this slightly lower reddening. Seaton's (1979) reddening curve is used to correct the observed fluxes to their unreddened values.

5.1 Forbidden lines

The [O I] lines at 5577, 6300 and 6363 Å, and [N II] 5577-Å lines are clearly present. Their profiles (Fig. 4) are almost flat-topped, but a central minimum is probably present. Since these lines are most probably optically thin, the profiles reflect the velocity distribution of the emitting gas. These forbidden lines are diagnostics of this gas. In the following analysis we consider the entire line profile and do not attempt to treat the blue and red components separately. From Table 1 we can say that the blue and the red components of the emission lines are symmetric. [O I] and [N II] emission indicate the presence of a nebula around the star. The overall symmetry and similarity of the profiles suggests that the physical conditions of the 'blue' and 'red' gas are not very different.

In considering the [O I] lines, we assume the 6363-Å line to have its predicted flux (which is one-third of the observed flux of the stronger 6300-Å line); the 6363-Å line is present but difficult to measure accurately. Then, the flux ratio is

$$F[\mathrm{O\ I}]=\frac{F(6300)+F(6363)}{F(5577)}=1.9\pm0.3.$$

Here, $F(\lambda)=W(\lambda)F_c(\lambda)$, where $F(\lambda)$ is the flux in the line, $W(\lambda)$ is the equivalent width and $F_c(\lambda)$ is the continuum flux corrected for interstellar reddening.

The isoelectronic ion N^+ has an analogous flux ratio involving the 5755-Å line, which is strong and readily measured (Fig. 4), and the line pair 6548 and 6583 Å. Unfortunately, the latter pair are blended with other lines: 6548 Å is blended with an Fe I line and 6583 Å with a C II line. A rough estimate of the flux in the 6548- and 6583-Å lines is made in the following way. The redward component of the 6548-Å line can be seen and measured. We assume that the blue component has the same strength, a symmetry clearly satisfied by the majority of the emission lines (see Table 1 and Figs 4–6). Since the relative strength of the 6583- to the 6548-Å line is fixed by their Einstein A coefficients, the total

Table 1. Emission lines.

λ	Ident.	Equiv.Width[a] (mÅ) blue	red	Flux[b]	Rad. vel. ($km\ s^{-1}$)	Base width ($km\ s^{-1}$)
6562.83	HI	1689	1612	3.5	-94.0	214.0
5875.63	HeI			5.5	-95.0	346.0
6678.15	HeI			3.3	-100.0	366.0
6707.78	LiI	195		3.3		139.0
5969.33	CI	65	35	5.1	-90.0	118.0
5805.19	CI	59	64	5.8	-90.0	130.0
5800.59	CI	100	109	5.8	-95.0	142.0
6855.55	CI	52	64	3.1	-87.0	134.0
6828.12	CI	237	246	3.1	-91.0	137.0
6655.51	CI	131	79	3.3	-90.0	149.0
6016.45	CI	54	37	4.9	-93.0	129.0
6001.13	CI	49	32	5.0	-91.0	136.0
6013.22	CI	52	82	4.9	-89.0	132.0
6663.04	CI	54	83	3.3	-99.0	145.0
6688.79	CI	43	42	3.3	-91.0	131.0
6671.84	CI			3.3	-99.0	212.0
6662.73	CI	47	75	3.3	-85.0	141.0
6100.46	CI	71	48	4.6	-94.0	128.0
6583.45	[NII]			3.5		
5754.80	[NII]	316	232	6.0	-106.0	140.0
6548.08	[NII]		40	3.5		
6300.23	[OI]	312	312	4.1	-81.0	115.0
6363.88	[OI]			4.0	-102.0	125.0
5577.35	[OI]	109	99	7.0	-89.0	125.0
6163.59	NeI			4.4		
6506.53	NeI			3.6		
6074.34	NeI			4.7		
6030.00	NeI			4.9		
6334.43	NeI			4.0		
6143.06	NeI			4.5		
6402.25	NeI			3.8		
6351.86	NeI			3.9		
5881.89	NeI			5.4		
5889.95	NaI			5.4		
5895.92	NaI			5.4		
5528.41	MgI	93	95	7.2	-89.6	135.0
5978.97	SiII	184	172	5.0	-94.0	190.0
6347.09	SiII	532	541	3.9	-103.0	195.0
6572.78	CaI	177		3.5		102.0
6122.23	CaI	122		4.6		144.0
6439.07	CaI	176		3.7		104.0
5956.70	FeI	180	225	5.1	-73.0	150.0
5501.47	FeI	92	87	7.4	-77.0	130.0
5497.52	FeI	59	38	7.4	-98.0	95.0
5506.78	FeI	35	38	7.4	-80.0	100.0
6318.02	FeI	484	500	4.0	-100.0	170.0
6191.56	FeI	90	70	4.4	-113.0	125.0
6270.24	FeI	195	130	4.1	-103.0	135.0
5615.65	FeI	73	54	6.7	-97.0	105.0
5586.76	FeI	65	70	6.9	-80.0	115.0
5624.55	FeI	37	26	6.7	-100.0	130.0
6432.65	FeII	637	576	3.8	-92.0	135.0
6516.05	FeII	688	761	3.6	-92.0	153.0
6129.71	FeII	123	142	4.5	-92.0	120.0
5991.38	FeII	475	474	5.0	-92.0	130.0
6084.11	FeII	276	269	4.7	-92.0	130.0
6113.33	FeII	165	140	4.6	-92.0	135.0
6116.04	FeII	74	69	4.6	-92.0	125.0
5534.86	FeII	375	368	7.2	-92.0	140.0
5525.40	FeII	95	105	7.3	-100.0	120.0
5627.49	FeII	116	122	6.7	-92.0	120.0
6456.38	FeII	842	746	3.7	-92.0	170.0
6247.56	FeII	290	320	4.2	-95.0	140.0
6147.74	FeII			4.5	-92.0	140.0
6416.91	FeII	284	406	3.8	-92.0	140.0
6149.24	FeII			4.5	-90.0	140.0
6407.30	FeII	125	226	3.8	-92.0	140.0
6219.54	FeII	256	198	4.3	-75.0	140.0
6179.38	FeII	91	107	4.4	-92.0	120.0
5813.67	FeII	103	90	5.7	-92.0	151.4
6482.21	FeII	53	64	3.7	-80.0	160.0
6331.97	FeII	149	203	4.0	-95.0	120.0
6175.16	FeII			4.4	-92.0	145.0
6103.54	FeII	173	112	4.6	-90.0	130.0
6627.28	FeII	217	228	3.4	-100.0	135.0
6108.12	NiI	79		4.6		133.0
6767.78	NiI	158		3.2		127.0

[a] The numbers refer to the blue and red components.
[b] Continuum flux–units: W cm^{-2} $\mu m^{-1} \times 10^{-17}$.

flux in the pair of lines is obtained by this procedure. The flux ratio is

$$F[\mathrm{N\ II}] = \frac{F(6548)+F(6583)}{F(5755)} = 0.45 \pm 0.15.$$

Osterbrock (1989) provides predictions of F(N II) as a function of the temperature (T) and electron density (n_e) of the emitting gas. A solution for the population of the various levels of [O I], and the relative line strengths emitted by them, was formulated along the lines of the discussion in Osterbrock (1989). The numerical values of the collision strengths and transition probabilities for [O I] were taken from Mendoza (1983). Fig. 7 represents the $\log(n_e)$–T plane for flux ratios of [O I] (solid lines) and [N II] (broken lines). The common region represents the range of solutions as $n_e = (3\text{–}7) \times 10^6$ cm^{-3} for $T = 8500$–$20\,000$ K.

5.2 Fe I and Fe II lines

The relatively large number of measurable Fe I and Fe II lines encouraged us to determine their excitation temperatures (T_{exc}). Extraction of T_{exc} from a set of line fluxes is straightforward for lines emitted by optically thin gas. Jeffery et al. (1988) suggested, however, that the gas emitting the Fe II lines was optically thick. This suggestion was prompted largely by their interpretation of the central minimum as a self-reversal. We consider the emitting gas to be optically thin if lines from a single multiplet scale with their Einstein A coefficients. In the optically thin limit, the line flux is given by

$$\log[W(\lambda)F_c(\lambda)] - \log gf + 3\log\lambda = \log N_2/g_2 + \log C;$$

let

$$\log[W(\lambda)F_c(\lambda)] - \log gf + 3\log\lambda = G,$$

where $W(\lambda)$ is the equivalent width, $F_c(\lambda)$ is the continuum flux corrected for interstellar reddening, N_2 is the upper level population and g_2 the statistical weight of that level, and C is a constant. Within a multiplet, the left-hand side of the above expression should be fairly constant unless the gas is optically thick or the excitation is exceptionally peculiar (i.e., selective fluorescence is involved). The left-hand side

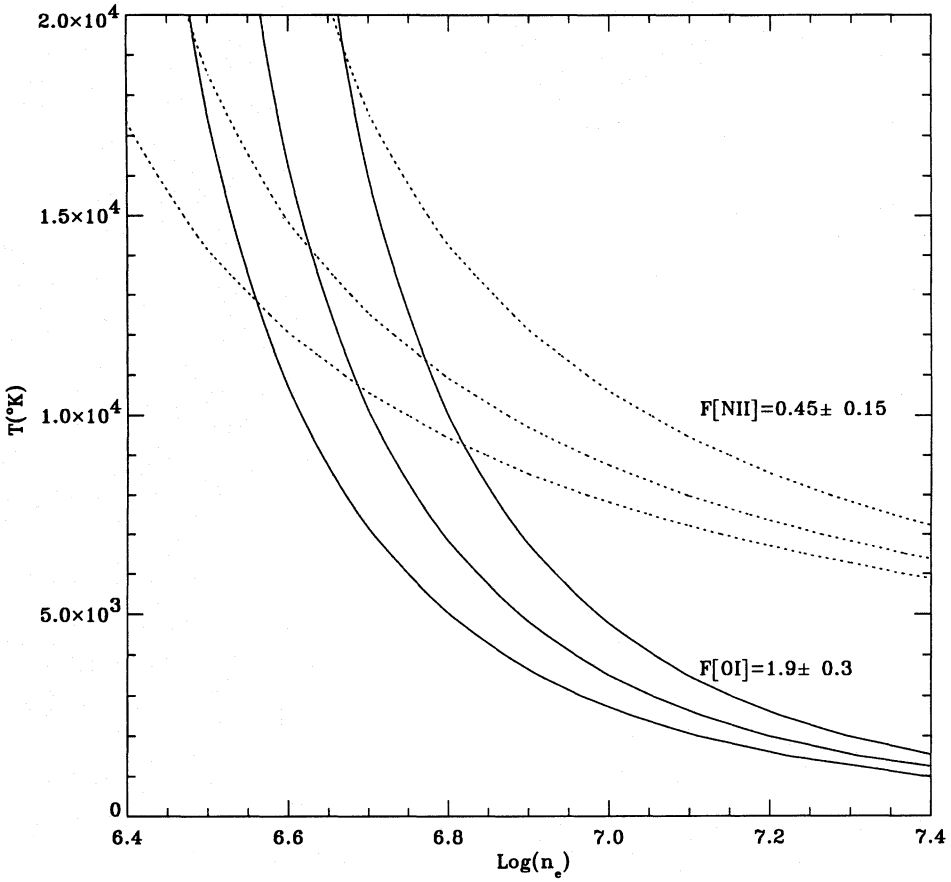

Figure 7. The log (n_e)–T plane showing the loci corresponding to the flux ratios F[N II] and F[O I] –see text. A combination $T \sim 1.5 \times 10^4$ K and log (n_e) ~ 6.6 satisfies the two observed ratios.

will not be constant if the lines come from optically thick gas for which the line flux may be almost independent of the *gf* values.

Four lines of the strong Fe II multiplet RMT46 in the red are shown in Fig. 6. By inspection it may be seen that the equivalent widths (hence, the line fluxes for these lines of similar wavelength) vary greatly across the multiplet, as would be expected for optically thin lines. This qualitative indicator of optical thinness is readily transformed to a quantitative measure by computing the left-hand side of the above expression G. We adopt the *gf* values given by Giridhar & Ferro (1995); the range in log *gf* is from -3.74 for the strongest line (5991 Å) to -4.56 (6116 Å). We perform the test separately on the blue and red components of the lines by computing G(blue) and G(red) for each line. In arbitrary units, we find values G(blue) of 1.45, 1.44, 1.55 and 1.45 for the lines in order of largest to smallest *gf*. Similarly for G(red), the values are 1.45, 1.43, 1.47 and 1.42. That the values within a multiplet are equal to within the measurement errors (say ± 0.1 dex) is evidence that the emitting gas is optically thin to the lines; log *gf* spans a range of 0.82 dex across these lines and G would vary by about this amount if the gas were optically thick.

The excitation temperature T_{exc} is provided by plotting G versus the excitation potential of the upper level (χ). This plot for the Fe II lines is shown in Fig. 8 where measurements from 6 multiplets are combined and the excitation potential (χ) spans about 4 eV. Blue and red components of the lines are shown separately. The line fitted to the points corresponds to $T_{exc} = 7400 \pm 400$ K. The same temperature fits the red and blue components. The *gf* values are again taken from Giridhar & Ferro (1995). The corresponding plot for the measurable Fe I lines is shown in Fig. 9 for which the *gf* values were taken from Giridhar & Ferro (1989) and the estimated excitation temperature is $T_{exc} = 4850 \pm 400$ K. Since the Fe I profiles are not so obviously double, we show the plot for the integrated line profile. These results fully confirm Herbig's (1975a) suggestion about excitation and colour temperatures.

The total number of Fe^+ ions is calculable, assuming that the excitation temperature applies to the unobserved and populous low-lying levels. If the same temperature is assumed for the Fe I lines, the ratio $N(Fe^+)/N(Fe)$ gives $n_e = 9 \times 10^7$ cm^{-3} when Saha's equation is adopted with $T = 7300$ K. If $T = 5000$ K is assumed for the excitation and ionization, $n_e = 2 \times 10^5$ cm^{-3} is found. These estimates indicate the lower and the upper limits on the electron density of the emitting regions. The [N II] and O I] lines give us an estimate of electron density which agrees well with the estimated range of electron density from Fe lines.

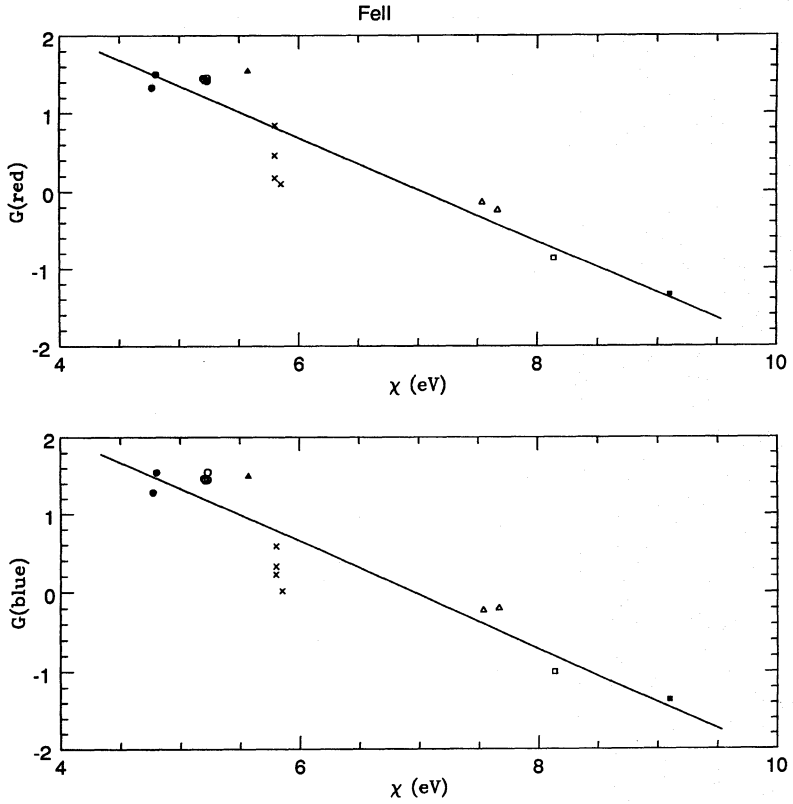

Figure 8. Excitation of the Fe II red and blue emission-line components. See text for definition of G. χ is the excitation potential of the upper level responsible for an emission line. Filled circles represent RMT40, open circles represent RMT46, crosses represent RMT47, open triangles represent RMT163, open squares represent RMT199, filled squares represent RMT210 and filled triangles represent RMT57.

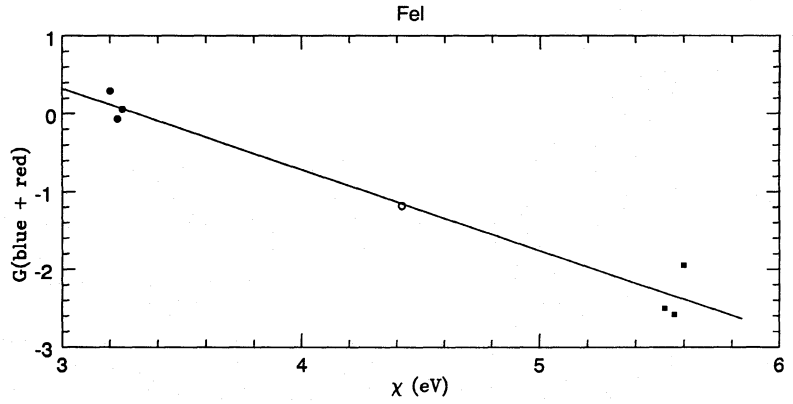

Figure 9. Excitation of the Fe I red and blue emission-line components. See text for definition of G. χ is the excitation potential of the upper level responsible for an emission line. Filled circles represent RMT15, open circles represent RMT169 and filled squares represent RMT686.

5.3 Li I emission at 6707 Å

A novel aspect of this study is the discovery of emission at 6707.8 Å corresponding to an Li I resonance doublet. No plausible alternative identification has been found. With the presence of Na I, Ni I, Ca I and other low-excitation lines in emission, the identification of Li I looks secure. The shape and width of the Li I profile closely resembles that of the other low-excitation lines.

An estimate of the abundance of Li/Ca can be made by using the Ca I intercombination line at 6572 Å. We assume that the emitting gas is optically thin to both lines. Certainly the profiles are similar in shape and are also quite similar to the profiles of stronger lines from more abundant elements. If the excitation temperatures are taken to be similar, the observed flux ratio with the well-determined Einstein A coefficients of the lines gives $\log N(\text{Li I})/N(\text{Ca I}) = -4.2$. Since Li and Ca atoms have similar first ionization poten-

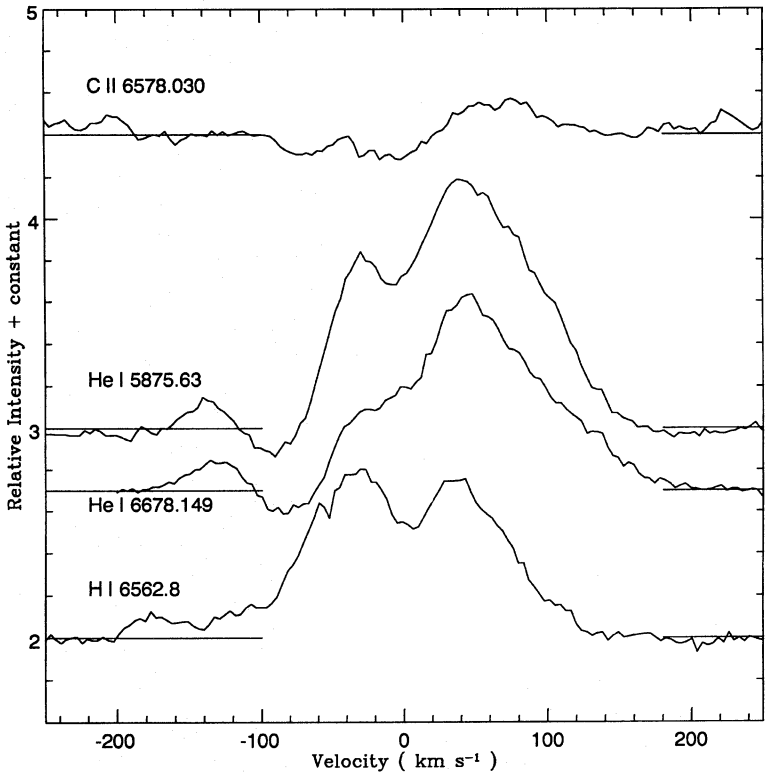

Figure 10. Comparison of emission-line profiles of high-excitation lines of C II, He I and Hα. The velocity scale is similar to Fig. 4. The mean continuum for each spectrum segment is marked as in Fig. 3.

tials, we assume the abundance ratio of the neutral atoms is the elemental abundance ratio. If the Ca abundance is the solar value, log Li = 2.1 for MV Sgr on the usual scale on which log H = 12.0. Compared to the solar abundance, the sulphur and silicon abundances determined by Jeffery et al. (1988) are deficient by 0.7 dex; if Ca is also deficient to the same extent, then log Li = 1.5. Solar Li abundance is 3.13 (from meteorites).

5.4 Hα, He I and C II profiles

Profiles of Hα, the He I λλ 5875 and 6678, and the C II λ6578 line are shown in Fig. 10. These emission profiles are considerably broader than those of Fe II and other lines; the emission in the red wing extends to about 100 km s^{-1} in contrast to 50 km s^{-1} for the Fe II lines. This difference suggests that Hα and the other lines come in large part from gas that is moving faster than that providing the Fe II and similar lines.

Another difference between He I and C II lines and the Fe II family of lines is the presence, in the former profiles, of blueshifted absorption. The He I lines show an absorption component at a relative velocity of about −80 km s^{-1} apparently superimposed on the broad emission. The C II λ6578 profile may also show an absorption component at −20 km s^{-1} relative to the stellar velocity. This may be, in part, the photospheric absorption line filled in by emission. It is likely that both He I and C II lines are affected by photospheric absorption. The blueshifted absorption in a symmetric emission profile is indicative of line formation in a stellar wind.

5.5 Variation of the emission width with excitation potential

The base width of the emission lines increases with excitation potential. Most of the emission lines are symmetrical about the stellar velocity. Fig. 11 shows the base width (mean base width of blue and red components) versus the excitation potential of the upper level: the higher the excitation potential, the broader the emission line. This could be a signal that the gas close to the star (high-excitation lines) is moving (rotation or expansion?) faster than the gas at greater distances (resonance and forbidden lines). An apparent exception is provided by the Na I D lines, which have a larger blue component width (1200 km s^{-1}) than do other resonance lines, for which a width of 60 km s^{-1} is representative. We suppose this difference reflects the higher optical depth in the Na D lines relative to the weak resonance (e.g., the Ca I] 6572 Å) or to the low-excitation lines providing the points in Fig. 11.

6 DISCUSSION

The double-peaked Fe II (and other) emission lines suggest that the emitting gas is confined either to a rotating envelope or to a bipolar flow. In both models the more excited lines are presumed to come from the inner regions closest to the star, where the rotation velocities or the wind velocities are highest. Keplerian motion about MV Sgr seems a feasible explanation for the velocity separation of the emission lines and the red and blue components. The expected Keplerian velocities are v (in km s^{-1}) $\simeq 120 R_h^{-0.5}$, where R_h

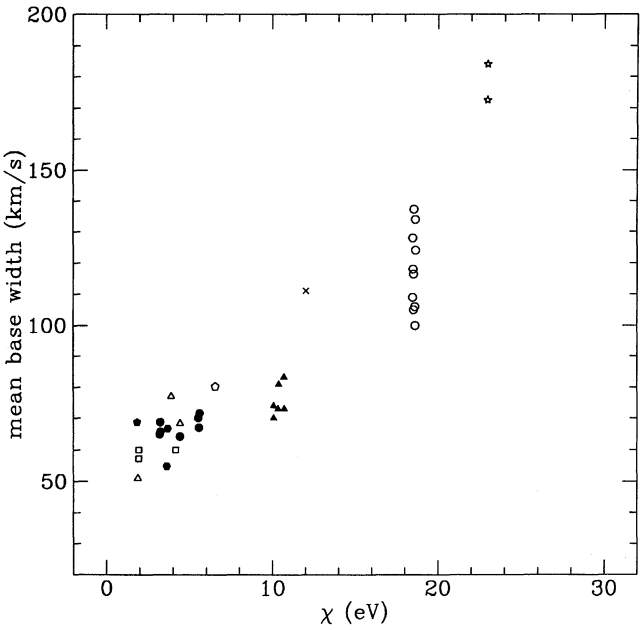

Figure 11. The mean base width of emission lines versus the excitation potential of an upper level of a line (χ in eV). Filled circles represent Fe I, open circles represent Ne I, open squares represent [O I], filled triangles represent C I, open triangles represent Ca I, cross represents H I, stars represent He I, filled pentagon represents Li I, open pentagon represents Mg I and filled hexagon represents Ni I.

is the distance from the stellar centre expressed in stellar radii. We estimate the stellar radius to be $R_* \simeq 13\ R_\odot$ from the assumptions that $M_{\rm bol} \simeq -5$ and $T_{\rm eff} \simeq 15\,000$ K. A circular velocity of ± 30 km s^{-1}, the displacement of the blue and red peaks, is attained at $R_h \sim 15R_*$. The observed separation includes an unknown projection factor so $R_h \leq 15R_*$ is suggested. This gas is well inside the dusty region responsible for the infrared emission characterized by the 1600-K blackbody, where $R_{\rm dust} \sim 40R_*$ (Walker 1985). The fact that the strong emission lines appear doubled suggests that, if the line splitting is due to rotation, the emitting gas is in a flattened system. In turn, this may suggest there is a preferred direction for outflow from the star.

In considering alternatives to a rotating envelope, the two (optically thin) peaks of the emission profiles could simply imply (indicate) two flows in different directions, towards and away from the observer irrespective of the presence of the dust disc (or torus), as long as the projected size of the dust disc is small compared to the resulting flow size. The most highly excited lines (e.g. He I) may sample the inner volume between the star and the disc, and receding gas on the 'far' side of the disc may be visible. This may account for the larger widths of these highly excited lines. The blue-shifted absorption in the He I and C II lines is probably formed close to the star, where the wind is fastest. This model, in which one component of the dust, presumably the warmer component ($T = 1600$ K), is concentrated into a disc, implies a preferred direction for the ejection of the gas and dust. The colder dust may be more spherically distributed.

7 CONCLUDING REMARKS

Our radial velocity, derived from the photospheric absorption lines, is consistent with the earlier measurements suggesting that MV Sgr is not a radial velocity variable: if it pulsates, it does so with a small amplitude; if it is a spectroscopic binary, the velocity amplitude of the visible star is small.

The emission-line spectrum shows that MV Sgr supports a wind: the He I lines show blueshifted absorption at an expansion velocity of about 80 km s^{-1}. The line profiles of other lines, from strong Fe II lines to weaker forbidden lines, are centred on the stellar velocity with a width that is an increasing function of excitation potential. We tentatively associate the emission lines with two flows, towards and away from the observer. We cannot exclude the possibility that the emitting gas is concentrated in a rotating (dust-free) torus. It seems possible that measurements of polarization will be helpful in refining the model.

A novel result of our study is the detection of the Li I resonance feature at 6707 Å in emission. We infer an abundance ratio Li/Ca, using the Li I 6707-Å and the Ca I 6752-Å intercombination line. If, as the Fe I and Fe II lines suggest, the excitation is quasi-thermal, we find $\log N({\rm Li\ I})/N({\rm Ca\ I}) = -4.2$, and the similarity of ionization potentials suggests that this is also the elemental ratio $\log N({\rm Li})/N({\rm Ca})$. If the calcium abundance of the star is solar, we find $\log {\rm Li} = 2.1$ on the usual scale. Since all stars prior to the onset of He core burning destroy or dilute the Li in their outer envelopes to a level well below this abundance, we must suppose that MV Sgr was able to resynthesize Li. Lithium production is observed and predicted to occur in the envelopes of intermediate-mass stars at high luminosities on the asymptotic giant branch (cf. Sackmann & Boothroyd 1992; Smith et al. 1995). The raw material for Li production is the ^{3}He synthesized on the main sequence; since the initial step of ^{3}He production from hydrogen is controlled by a very slow weak reaction, the main-sequence phase for low-mass stars seems to be the sole practical site for ^{3}He synthesis. In principle, the ^{3}He may be processed to ^{7}Li at other sites and other stages of evolution; for example, Podsiadlowski, Cannon & Rees (1995) suggest that ^{7}Li production occurs in a Thorne–Żytkow object, a red giant with a neutron star as its core. We suppose that MV Sgr has evolved from an intermediate-mass AGB star, and that possibly the Li was produced in the final He thermal flash after the star had left the AGB to enter the white dwarf cooling track.

The abundance analysis of Jeffery et al. (1988) suggests that N is more abundant than C, a situation different from other hot hydrogen-deficient stars. The super-Li-rich AGB stars observed by Smith and Lambert in the LMC are of high luminosities ($M_{\rm bol} \sim -6.5$) and show N to be more abundant than C. This has been interpreted as a conseqeunce of C from the helium burning being further processed by CNO cycles to N (Sackmann & Boothroyd 1992). If such a star were to evolve to hotter regions and become hydrogen deficient, it would probably show similar abundances to MV Sgr.

Lithium is not an unknown ingredient of RCBs. In four out of 18 stars [the warm RCBs ($T_{\rm eff} \simeq 5000$–8000 K)], Lambert & Rao (1994) report lithium to be present and

with an abundance similar to that inferred for MV Sgr. Lithium in the small sample of hydrogen-deficient cool carbon stars is found in one of five stars in the sample. Of course, lithium will not be detectable in hot RCBs unless these stars possess cooler absorbing/emitting regions, as is the case for MV Sgr.

Of the many questions unanswered by our study, we expect to answer a few by extending high-resolution spectroscopy across the visible spectrum and beyond. High signal-to-noise ratio spectra will surely reveal additional details about the line profiles. Spectra in the blue may show lines of heavy elements which should be enhanced if MV Sgr has evolved from an AGB star. The lighter elements, say Ge–Mo, should be severely enhanced if MV Sgr is a Thorne–Żytkow object (Biehle 1991, 1994; Cannon 1993).

The authors thank the referee, Simon Jeffery, for his valuable comments. This research has been supported by an International Travel Grant from the US National Science Foundation. DLL thanks the NSF for additional support through grant AST-93315124.

REFERENCES

Appenzeller L., Jankovics I., Ostreicher R., 1984, A&A, 141, 108
Biehle G. T., 1991, ApJ, 380, 167
Biehle G. T., 1994, ApJ, 420, 364
Cannon R. C., Eggleton P. P., Żytkow A. N., Podsiadlowski P., 1992, ApJ, 386, 206
Drilling J. S., Schönberner D., Heber U., Lynas-Gray A. E., 1984, ApJ, 278, 224
Feast M. W., Glass I., 1973, MNRAS, 161, 293
Giridhar S., Arellano Ferro A., 1989, JA&A, 10, 47
Giridhar S., Arellano Ferro A., 1995, Rev. Mex. Astron. Astrofis., 31, 23
Heber U., Schönberner D., 1981, A&A, 102, 73
Herbig G. H., 1964, ApJ, 140, 1317
Herbig G. H., 1975a, ApJ, 199, 702
Herbig G. H., 1975b, ApJ, 196, 129
Hoffleit D., 1958, AJ, 63, 50
Jeffery C. S., Heber U., Hill P. W., Pollacco D., 1988, MNRAS, 231, 175
Kilkenny D., Whittet D. C. B., 1984, MNRAS, 208, 25
Krelowski J., 1989, in Allamandola L. J., Tielens A. G. G. M., eds, Interstellar Dust. Kluwer, Dordrecht, p. 67
Lambert D. L., Rao N. K., 1994, JA&A, 15, 47
Landolt A. R., 1979, IAU Circ. No. 3419
Mendoza C., 1983, in Flower D. R., ed., Proc. IAU Symp. No. 103. Reidel, Dordrecht, p. 143
Osterbrock D. E., 1989, Astrophysics of gaseous nebulae and active galactic nuclei. University Science Books, Mill Valley, California
Podsiadlowski P., Cannon R. C., Rees M. J., 1995, MNRAS, 274, 485
Rao N. K., Nandy K., 1982, JA&A, 3, 79
Rao N. K., Houziaux L., Giridhar S., 1990, JA&A, 11, 37
Sackmann I.-J., Boothroyd A. I., 1992, ApJ, 392, L71
Seaton M. J., 1979, MNRAS, 187, 735
Smith V. V., Plez B., Lambert D. L., Lubowich D. A., 1995, ApJ, 441, 735
Walker H. J., 1985, A&A, 152, 58
Walker H. J., 1986, in Proc. IAU Colloq. No. 87. Reidel, Dordrecht, p. 407